MNRAS 000, 1–7 (2019) Preprint 10 January 2019 Compiled using MNRAS LATEX style file v3.0

The Globular Cluster System of the Auriga Simulations

Timo L. R. Halbesma[1★], Philipp Busch[1], Wilma Trick[1], Robert J. J. Grand[1], Volker Springel[1], Facundo A. Gómez[2,3], Federico Marinacci[4,5], Rüdiger Pakmor[1], Simon D. M. White[1]

[1] *Max-Planck-Institut für Astrophysik, Postfach 1317, D-85741 Garching, Germany*
[2] *Instituto de Investigación Multidisciplinar en Ciencia yTecnología, Universidad de La Serena, Raúl Bitrán 1305, La Serena, Chile*
[3] *Departamento de Física y Astronomía, Universidad de La Serena, Av. Juan Cisternas 1200 N, La Serena, Chile*
[4] *Department of Physics, Kavli Institute for Astrophysics and Space Research, MIT, Cambridge, MA 02139, USA*
[5] *Harvard-Smithsonian Center for Astrophysics, 60 Garden Street, Cambridge, MA 02138, USA*

Accepted XXX. Received YYY; in original form ZZZ

ABSTRACT

We investigate whether the galaxy formation model used for the Auriga simulations can produce a realistic globular cluster population at redshift zero. We compare properties of the simulated star particles in the Auriga haloes with catalogues of observations of the Milky Way globular cluster population available in the literature. We find that the Auriga simulations produce sufficient mass at radii and metallicities that are typical for the MW GCS, although we observe a varying mass-excess for the different r_{gal}-[Fe/H] bins. This implies different values for the combined product of the bound cluster formation efficiency and the globular cluster disruption rate. We investigate wether these differences could result from formation insitu vs. accreted star particles. We find ...

Key words: methods: numerical – galaxies: formation – galaxies: star clusters: general.

1 INTRODUCTION

Paragraph: General introduction of GCs

Diemand et al. (2005): "The radial profile of the stellar halo and metal-poor globular clusters of the Milky Way suggest that these components formed in rare early peaks above 2.5σ at redshift above 10. "

Renaud et al. (2017): "GCs among oldest astrophysical objects. GCs form in the early Universe in highest density peaks (e.g. Diemand et al. 2005; Boley et al. 2009)"

- "Hence, they witness most of the formation and evolution processes of galaxies, and can be used to probe them" (Brodie & Strader 2006)
- "colour bimodality, blue and red clusters (e.g. Zinn 1985; Gebhardt & Kissler-Patig 1999; Larsen et al. 2001; Peng et al. 2006)
- "blue metal-poor (with distribution peaking at [Fe/H] ≈ -1.5 for the Milky Way), no sign of rotation as a population (..) more metal-rich (peak at [Fe/H] ≈ -0.5 in the Milky Way) more spatially concentrated and rotating with the galaxy." (Harris 1996)

Paragraph: "Bimodality suggests two formation mechanisms". In-situ vs. Accreted

- "Blue clusters from in early Universe in galaxies that merge later. In (wet) merger process starbursts generate red population Ashman & Zepf (1992); Schweizer (1987)"
- "Forbes et al. (1997) propose instead that blue globulars form when the protogalaxy itself collapses, in a metal-poor and turbulence media. The red population would form later, once the galactic disc has settled. The formation of globular clusters would then be a multiphase process, with the first phase being interrupted possibly by cosmic reionization (Beasley et al. 2002)."
- "Kravtsov & Gnedin (2005); Li & Gnedin (2014) advocate that major mergers are at the origin of both sub-populations: blue clusters form during early mergers (z > 4) while the red ones appear in mergers at lower redshifts (even after z = 1). Although, this scenario, combined with star formation enhancement in mergers, seems appropriate in dense galactic environment leading to the assembly of massive elliptical galaxies, like in the Virgo Cluster as tested by Li & Gnedin (2014), it does not apply to Milky Way-like systems where no recent major merger took place (Wyse 2001; Deason et al. 2013; Ruchti et al. 2014, 2015).
- "Côté et al. (1998) argue that red clusters form in situ while the blue ones are accreted, either via merging satellite galaxies, or by tidal capture of the clusters themselves (see also Tonini 2013)."

Dark Matter - GC connection

Paragraph: scientific motivation

★ E-mail: Halbesma@MPA-Garching.MPG.DE

- The star formation model implemented in the Auriga simulations is capable of producing a suite/population of realistic Milky Way-like galaxies at redshift zero.
- (However) State of the art simulations still face numerical restrictions that requires a subgrid approach to star formation and feedback because individual stars (and their evolution) cannot yet be accounted for. Star formation thus occurs in a heuristic/probabilistic fashion for gas cells that fulfill some star formation criterion. The star particles enrich the gas with metals and energy, both according to pre-defined/pre-calculated yields for specific feedback processes (supernova type I and II, strong stellar winds of asymptotic giant branch stars,). In addition, black holes are seeded in eligible haloes to account for feedback associated with an active galactic nucleus.
- The end-result of the star formation model is the production of simulated Milky Way-like galaxies. Therefore the question naturally arises whether or not the Auriga simulations are also capable of faithfully producing a globular cluster population as observed in the Milky Way.
- Globular cluster formation in cosmological zoom simulations is very interesting for two reasons. First of all, extragalactic observations typically show the integrated properties of globular clusters rather than that of the individual stars within the clusters. Moreover, the typical mass scale of globular clusters is comparable to the numerical (mass) resolution of cosmological zoom simulations. The detailed small scale physics that is at play for real world globular clusters appears in observations as the combined effect of the 10^{3-6} $M_\odot$, compared to a mass resolution of 10^{3-5} $M_\odot$for the Auriga simulations. Globular clusters can therefore serve as an ultimate test to the star formation model that is implemented in the numerical simulations. Secondly, cosmological zoom simulations provide an accurate recording of the full and detailed merger history of the simulated galaxy. This is important because theoretical paradigms for globular cluster formation in the literature know two distinct classes of GCs that are separated by their exact formation sites: an in-situ versus an accreted population. Cosmological zoom simulations are uniquely allow for an investigation into globular cluster formation with particular focus on the in-situ and accreted populations.

Paragraph: previous work / work of other groups

This goes before the GC formation mechanism paragraph.

- Origin of the Milky Way globular clusters (Renaud et al. 2017)
- GCs in FIRE (Kim et al. 2018)
- EMOSAICS project (Pfeffer et al. 2018)
- Origin of GC bimodality? (Fernandez & Bryan 2018)
- *GAIA* DR2: GC kinematics (Gaia Collaboration et al. 2018), Dating GC Tidal Disruption (Bose et al. 2018)
- GC in N-body simulation (Carlberg 2018)
- Tangentially related? role of GC mass evolution on stream properties (Balbinot & Gieles 2018)
- GC formation from dwarfs to giants (Choksi et al. 2018)
- GC contribution to EOR (Boylan-Kolchin 2018)
- Early Universe supermassive star / GC formation (Gieles et al. 2018)
- GC formation in cold filaments (Mandelker et al. 2018)
- GC formation in high-redshift dwarf galaxies (Zick et al. 2018)
- GCs in MW outer region (Peebles 2017)
- Impact of the Cutoff of the Cluster Initial Mass Function (Choksi & Gnedin 2018)
- Metallicity gradients in the globular cluster systems of early-type galaxies: in situ and accreted components (Forbes & Remus 2018)
- Globular clusters in M31, Local Group, and external galaxies (Larsen 2016)
- Globular Clusters Formed within Dark Halos I: present-day abundance, distribution and kinematics (Creasey et al. 2019)
- The mass of the Milky Way from satellite dynamics (Callingham et al. 2018)
- Globular cluster formation and evolution in the context of cosmological galaxy assembly: open questions (Forbes et al. 2018)
- The kinematics of globular clusters systems in the outer halos of the Aquarius simulations (Veljanoski & Helmi 2016)
- Star Cluster Formation in Cosmological Simulations (Li et al. 2017, 2018; Li & Gnedin 2018)
- A systematic analysis of star cluster disruption by tidal shocks – I. Controlled N-body simulations and a new theoretical model (Webb et al. 2018)
- Spatial mixing of binary stars in multiple-population globular clusters (Hong et al. 2018)
- Star Clusters Across Cosmic Time (Krumholz et al. 2018)
- Kinematics of Subclusters in Star Cluster Complexes: Imprint of their Parental Molecular Clouds (Fujii 2018)
- Investigating the population of Galactic star formation regions and star clusters within a Wide-Fast-Deep Coverage of the Galactic Plane (Prisinzano et al. 2018)

Paper outline

We summarise the relevant characteristics of the Auriga simulations in section 2, followed by a summary of the observations of the Milky Way (MW) globular cluster system (GCS) in section 3 that we use to compare our simulations to in section 4. We discuss our findings in section 5 to come to our conclusions in section 6.

2 THE AURIGA SIMULATIONS

We use the Auriga simulations (Grand et al. 2017, hereafter G17), a suite of high-resolution cosmological zoom simulations ran with a galaxy formation model that produces realistic Milky Way-like galaxies at redshift $z = 0$. The simulations are performed with the state-of-the art code AREPO (Springel 2010; Pakmor et al. 2016) that solves the magnetohydrodynamical equations on a moving mesh.

The interstellar medium is modelled using a sub-grid approach which implements the physical processes most relevant to galaxy formation and evolution. This model was tailored to the AREPO code and calibrated to reproduce key observables of galaxies, such as the history of the cosmic star formation rate density, the stellar mass to halo mass relation, and galaxy luminosity functions.

The sub-grid includes primordial and metal-line cooling with self-shielding corrections. Reionization is completed at redshift six by a time-varying spatially uniform UV background (Faucher-Giguère et al. 2009; Vogelsberger et al. 2013) The interstellar medium is described by an equation of state for a two-phase medium in pressure equilibrium (Springel & Hernquist 2003) with stochastic star formation in thermally unstable gas with a density threshold of $n = 0.13 \mathrm{cm}^{-3}$, and consecutive stellar evolution is accounted for. Stars provide feedback by stellar winds (Marinacci et al. 2014; Grand et al. 2017), and further enrich the ISM with metals from SNIa, SNII, and AGB stars (Vogelsberger et al. 2013). The formation of black holes is modelled which results in feedback from active galactic nuclei (Springel et al. 2005; Marinacci et al. 2014; Grand et al. 2017). Finally, the simulations follow the evolution of a magnetic field of 10^{-14} (comoving) G seeded at $z = 127$ (Pakmor

& Springel 2013; Pakmor et al. 2014). See G17 for further details of the numerical setup as well as the galaxy formation model.

"The diversity in morphological properties of these simulated galaxies reflects the stochasticity inherent to the process of galaxy formation and evolution (e.g. Bullock & Johnston 2005; Cooper et al. 2010; Tumlinson 2010)."

2.1 Definition of stellar halo

Possibly also relevant here. See Monachesi et al. (2018).

2.2 Definition of accreted and in-situ component

Possibly also relevant here. See Monachesi et al. (2018).

3 RELEVANT OBSERVATIONAL DATA

The galaxy formation model implemented for the Auriga simulations produces realistic spiral galaxies at redshift zero. Therefore we aim to compare the simulations to the globular cluster systems of the spiral galaxies in the Local Group (i.e. the Milky Way and Andromeda galaxy or M31). Here we summarise the relevant data available in the literature.

3.1 Milky Way: Harris catalogue

Harris (1996, 2010 edition; hereafter H96) provides a fairly up-to-date, comprehensive catalogue of the Milky Way globular cluster system and contains properties of 157 globular clusters. The catalogue is believed to be roughly 90% complete. The relevant data fields that we use from H96 are the metallicity [Fe/H], galactocentric radius $r_{\rm gal}$, and absolute magnitude in the V-band M_V.

We use the latter to calculate a mass-estimate by assuming $M_{V,\odot}$ = 4.83 and a mass to light ratio M/L_V = 1.7 M/L$_\odot$ (the mean for MW clusters McLaughlin & van der Marel 2005).

In Fig. 1 we show a two-dimensional mass-weighted distribution, splitting the data up in bins of both radius and metallicity. Later on we investigate whether the star formation model implemented for the Auriga simulations can produce a sufficient total mass in globular cluster candidates at the right values of radius, metallicity, and radius-metals, see Sec. 4.3

3.2 Milky Way: VandenBerg catalogue

VandenBerg et al. (2013, hereafter V13) used photometric data to obtain [Fe/H] measurements and age-estimates for 55 globular clusters in the Milky Way. The mean value of the age-estimates in this data set is 11.9 ± 0.1 Gyr and the dispersion is 0.9 Gyr. Furthermore, only one of the 55 GC age-estimates is below 10 Gyr.

How is this particular sample selected? What biases does this introduce? Is this sample drawn from the same underlying distribution as the Harris sample (plot distributions of FeH, compare mean/std, do t-test)

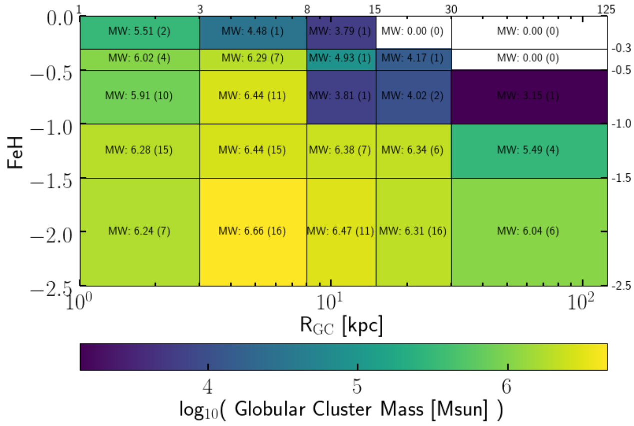

Figure 1. Mass-weighted $r_{\rm gc}$-[Fe/H] distribution of 151 GCs in the MW (data from Harris 1996, 2010 ed.), which is 98.19 % of the total MW GCS mass.

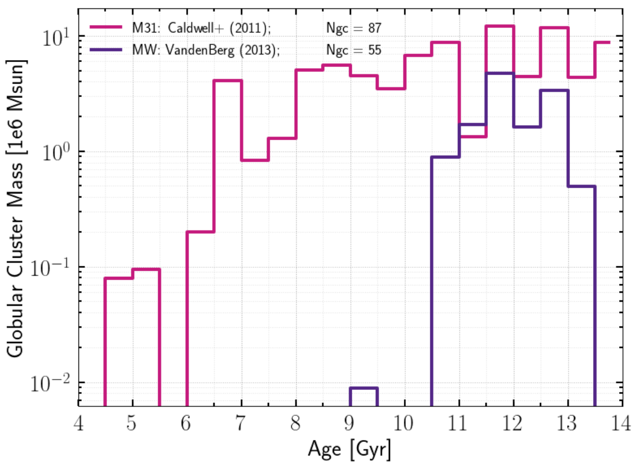

Figure 2. Mass-weighted age distribution of 55 GCs in the MW (data from VandenBerg et al. 2013) and 87 GCs in M31 (data from Caldwell et al. 2011).

3.3 Andromeda: Caldwell catalogue

Caldwell et al. (2011, , hereafter C11) studied globular clusters in the Andromeda galaxy. The relevant fields in this data set are the age, metallicities, and absolute visual magnitude.

'For M31 GC masses we combine the catalogues of Caldwell et al. (2011, using the given masses) and Huxor et al. (2014, again assuming M/L_V = 1.7 M/L$_\odot$, e.g. Strader, Caldwell & Seth 2011).'

For M31 we find an age distribution with a mean value of 10.8±10.8 Gyr and a dispersion of 2.3 Gyr. Furthermore, 27 GCs have age-estimates below 10 Gyr, and the minimum age is 4.8 Gyr. Perhaps an age cut of 6 Gyr would would be more appropriate for M31, see Fig. 2.

Furthermore, we supplement observational data of globular clusters in M31 with Huxor et al. (2014); Veljanoski et al. (2014)

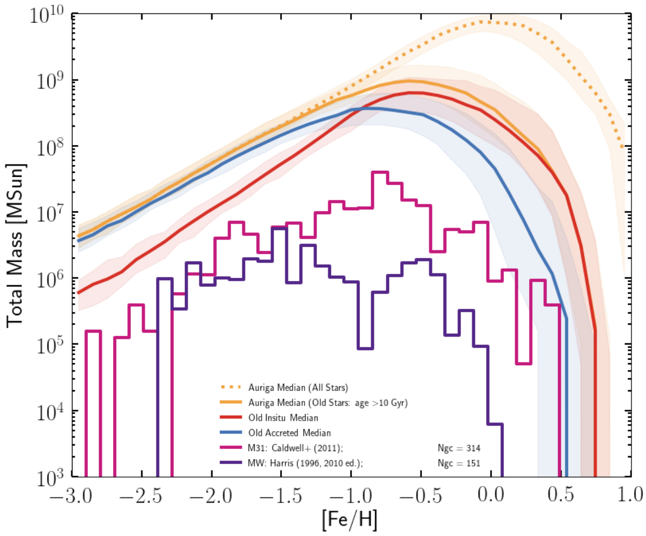

Figure 3. Mass-weighted metallicity distribution of star particles in the Auriga simulations. We show the median value of all Auriga haloes for all stars (orange dotted) and globular cluster candidates (i.e. stars with age > 10 Gyr; orange solid). The latter sub set is further split up between stars that formed in-situ (red solid), and those that were accreted (blue solid). Shaded regions indicate the 1σ interval. The MW GCS is shown in purple and that of M31 in pink. We use the same bin sizes for the simulations as for the observations, explicitly plotted for the observed profiles.

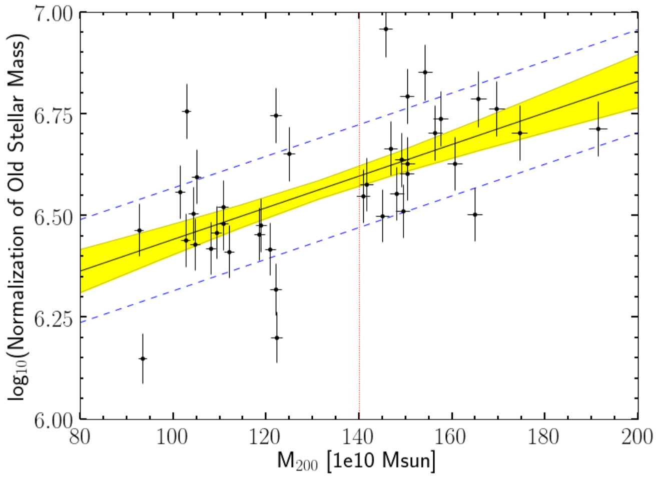

Figure 4. Plot of $\log_{10}$(mass normalization) [i.e. b obtained above] against the virial mass $M_{200,c}$ of the Auriga haloes. We fit a linear relation to see whether there is a correlation, and find $a = 0.00388$, $b = 6.597$. The red dotted line shows the 'central' value of $M_{200,c}$, the yellow region shows the 1σ interval around the best-fit relation, and the blue dashed lines shows the intrinsic scatter. The error bars show 1% of the obtained values.

4 RESULTS

We investigate globular cluster candidates in the Auriga simulations using an age cut to select of stars that formed at a lookback time greater than 10 Gyr. We chose this particular value because the mean age-estimate of the 55 in V13 is 11.9 ± 0.1 Gyr with a dispersion of 0.8 Gyr, and only one observed globular cluster falls below this selection criterion.

In Sec. 4.1 we investigate the metallicity distribution of the GC candidates, in Sec. 4.2 we show the distribution of galactocentric radii of the globular cluster candidates within the Auriga simulations, and we combine both in Sec. 4.3. We continue our analysis with a deeper analysis of the properties of the proto-galaxies at times of birth of the accreted globular cluster population in Sec. 4.4

4.1 Metallicity distribution

Can the Auriga simulations produce star particles of > 10 Gyr (GC candidates) with a metallicity distribution that is consistent with the MW GCS?

In Fig. 3 we show a mass-weighted metallicity distribution of star particles in the Auriga simulations. We show the median value of all Auriga haloes for all stars (orange dotted lines) and globular cluster candidates orange solid). The latter sub set is further split up between stars that formed in-situ (red solid), and those that were accreted (blue solid). The shaded regions indicate the 1σ interval. The MW GCS is shown in purple and that of M31 in pink. We use the same bin sizes for the simulations as for the observations, explicitly plotted for the observed profiles.

We find that the metallicity range $-3 <$ [Fe/H] < -1 is only populated by star particles older than ten Gyr, while [Fe/H] > -1 is dominated by star particles younger than 10 Gyr (with a difference of two orders of magnitude). Furthermore, the old accreted star particles contribute most significantly to the range $-3 <$ [Fe/H] < -1, and the contribution of the old in-situ star particles at these metallicities declines steeper with declining metallicity than the old accreted population. The old in-situ population provides the dominant contribution of the old population for [Fe/H] > -1.

We notice a scatter[1] in mass normalization of 0.3 dex between the different Auriga galaxies. We investigate whether there is a correlation between the total stellar mass in (old) star particles and the virial mass[2] $M_{200,c}$ of the host halo. We fit $a \cdot \left(M_{200,c}[1e10 M_\odot] - 140\right) + b$ to $\log_{10}\left(\Sigma_i m_i(_{[Fe/H]=-3})\right)$. Our fit thus provides the slope a and normalization of (old) stellar mass b at [Fe/H]=-3 for $M_{200,c}$ at 140e10 $M_\odot$. We find $a = 0.00388$, $b = 6.597$ and conclude that there is a small positive correlation of mass in (old) star particles with the virial mass of the host halo.

Furthermore we compare the simulated metallicity distribution to observations of the Milky Way and M31.

yes/no bimodal
M31 slope between -3 and -1 consistent with old insitu?
MW above 0 no more GCs, but Auriga well populated (mostly insitu, but also too many accreted.
should also comment on all vs old (Auriga simulation) btw

bla. Conclusion: too many metal-rich star particles.

4.2 Spatial distribution

Is the spatial distribution of the GC candidates in the Auriga simulations consistent with the MW GCS?

Look into Pandromeda survey. Star counts, very wide angle survey

[1] Here scatter means the width of the 1σ interval. The difference between the minimum and maximum values is 0.9 dex.

[2] The virial mass is defined as the mass contained inside the radius $r_{200,c}$ at which the average (spherical) mass density equals two hundred times the critical density of the Universe

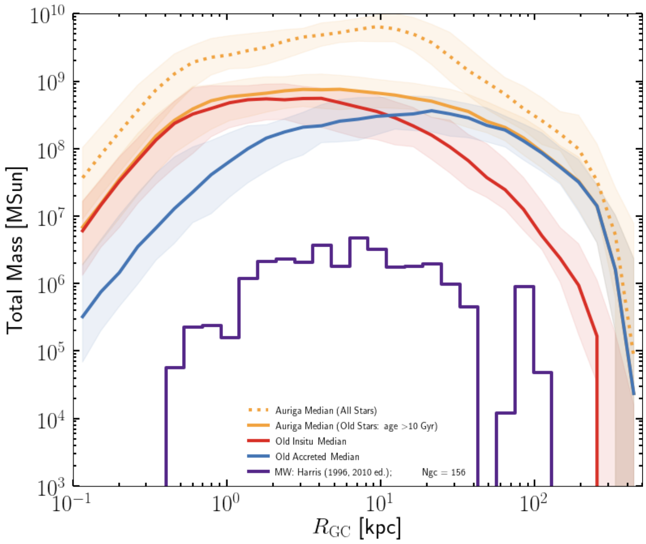

Figure 5. Mass-weighted distribution of galactocentric radii at which star particles in the Auriga simulations are found.

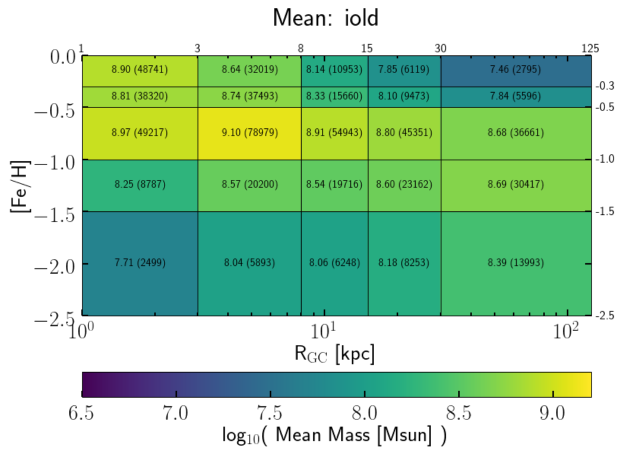

Figure 6. Mass-weighted [Fe/H]-r_{gc} distribution of all Auriga haloes (level 3, 4 and 5). Here we consider the old (> 10 Gyr) stars in all simulations and color-code the **mean value** (of 40 Auriga haloes)

4.3 Radius-metallicity distribution

What age-metallicity distribution is produced by star formation events in the Auriga simulations? ?

4.4 Properties of birth haloes of the accreted population

4.5 Age-metallicity distribution

What age-metallicity distribution is produced by star formation events in the Auriga simulations?

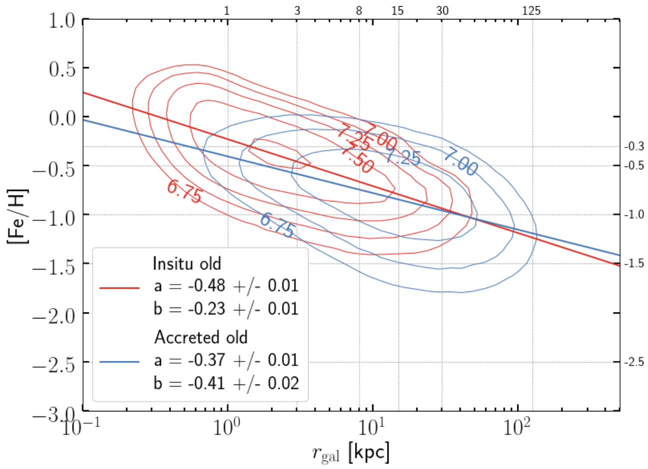

Figure 7. OMG what a beautiful plot - now only need 1σ interval around both relations, and need to know exactly what model I fit...

4.6 Mass budget

Does the star formation model implemented in the Auriga simulations produce sufficient mass in star particles with properties that are consistent with the MW GCS?

What efficiencies could we afford if we would take into account the combined mass loss effect of converting from star particles to bound star clusters and globular cluster disruption?

How does the total stellar mass in $r_{\mathbf{gal}}$-[Fe/H] bins compare to the MW GCS?

4.7 Formation history

Can we identify particular star formation events that generate GC candidates with the correct age, metallicity, and radial properties as expected or the MW GCS?

Can we distinguish between particles that have formed in-situ and those that have been accreted? Can we identify specific features in the age-metallicity plane, or in the $r_{\mathbf{gal}}$-[Fe/H] plane, that result from one of both populations? How does this connect to proposed mechanisms for globular cluster formation in the literature?

Orbits: are the pericentres different? Look at velocity + specific angular momentum distribution in the different FeH/Rgc bins as proxy for the pericenter

5 DISCUSSION

We investigate all star particles in the Auriga simulations that are older than 10 Gyr, an approach equal to the method of (Renaud et al. 2017). This approach does not take the bound cluster fraction (e.g. Kruijssen 2012) into account. This means that our sub set, which is based on selection by age, comprises both stars in the field as well as globular clusters. We compare the total mass in the simulations in metallicity ([Fe/H]), galactocentric radius $r_{\rm gc}$, and [Fe/H]-$r_{\rm gal}$ bins to the total mass in the MW GCS (using the H96 data set). The mass excess in the simulations gives a maximum mass loss 'budget' for the product of cluster formation efficiency and dynamical evolution. We find fractions that vary with metallicity, radius and metallicity-and-radius.

"The fraction of all star formation that occurs in bound stellar clusters (the cluster formation efficiency, hereafter CFE) follows by integration of these local clustering and survival properties over the full density spectrum of the ISM, and hence is set by galaxy-scale physics. We derive the CFE as a function of observable galaxy properties, and find that it increases with the gas surface density" (Kruijssen 2012)

6 SUMMARY AND CONCLUSIONS

ACKNOWLEDGEMENTS

TLRH acknowledges support from the International Max-Planck Research School (IMPRS) on Astrophysics.

Check Auriga boilerplate that we need to acknowledge

RG and VS acknowledge support by the DFG Research Centre SFB-881 'The Milky Way System' through project A1. This work has also been supported by the European Research Council under ERC-StG grant EXAGAL- 308037. Part of the simulations of this paper used the SuperMUC system at the Leibniz Computing Centre, Garching, under the project PR85JE of the Gauss Centre for Supercomputing. This work used the DiRAC Data Centric system at Durham University, operated by the Institute for Computational Cosmology on behalf of the STFC DiRAC HPC Facility 'www.dirac.ac.uk'. This equipment was funded by BIS National E-infrastructure capital grant ST/K00042X/1, STFC capital grant ST/H008519/1 and STFC DiRAC Operations grant ST/K003267/1 and Durham University. DiRAC is part of the UK National E-Infrastructure.

REFERENCES

Ashman K. M., Zepf S. E., 1992, ApJ, 384, 50
Balbinot E., Gieles M., 2018, MNRAS, 474, 2479
Beasley M. A., Baugh C. M., Forbes D. A., Sharples R. M., Frenk C. S., 2002, MNRAS, 333, 383
Boley A. C., Lake G., Read J., Teyssier R., 2009, ApJ, 706, L192
Bose S., Ginsburg I., Loeb A., 2018, ApJ, 859, L13
Boylan-Kolchin M., 2018, MNRAS, 479, 332
Brodie J. P., Strader J., 2006, ARA&A, 44, 193
Bullock J. S., Johnston K. V., 2005, ApJ, 635, 931
Caldwell N., Schiavon R., Morrison H., Rose J. A., Harding P., 2011, AJ, 141, 61
Callingham T., et al., 2018, arXiv e-prints,
Carlberg R. G., 2018, ApJ, 861, 69
Choksi N., Gnedin O. Y., 2018, arXiv e-prints,
Choksi N., Gnedin O. Y., Li H., 2018, MNRAS, 480, 2343
Cooper A. P., et al., 2010, MNRAS, 406, 744
Côté P., Marzke R. O., West M. J., 1998, ApJ, 501, 554
Creasey P., Sales L. V., Peng E. W., Sameie O., 2019, MNRAS, 482, 219
Diemand J., Madau P., Moore B., 2005, MNRAS, 364, 367
Faucher-Giguère C.-A., Lidz A., Zaldarriaga M., Hernquist L., 2009, ApJ, 703, 1416
Fernandez R., Bryan G. L., 2018, MNRAS, 479, 200
Forbes D. A., Remus R.-S., 2018, MNRAS, 479, 4760
Forbes D. A., Brodie J. P., Grillmair C. J., 1997, AJ, 113, 1652
Forbes D. A., et al., 2018, Proceedings of the Royal Society of London Series A, 474, 20170616
Fujii M. S., 2018, arXiv e-prints, p. arXiv:1812.01858
Gaia Collaboration et al., 2018, A&A, 616, A12
Gebhardt K., Kissler-Patig M., 1999, AJ, 118, 1526
Gieles M., et al., 2018, MNRAS, 478, 2461
Grand R. J. J., et al., 2017, MNRAS, 467, 179
Harris W. E., 1996, AJ, 112, 1487
Hong J., Patel S., Vesperini E., Webb J. J., Dalessandro E., 2018, MNRAS, p. 3147
Huxor A. P., et al., 2014, MNRAS, 442, 2165
Kim J.-h., et al., 2018, MNRAS, 474, 4232
Kravtsov A. V., Gnedin O. Y., 2005, ApJ, 623, 650
Kruijssen J. M. D., 2012, MNRAS, 426, 3008
Krumholz M. R., McKee C. F., Bland-Hawthorn J., 2018, arXiv e-prints, p. arXiv:1812.01615
Larsen S. S., 2016, in Bragaglia A., Arnaboldi M., Rejkuba M., Romano D., eds, IAU Symposium Vol. 317, The General Assembly of Galaxy Halos: Structure, Origin and Evolution. pp 120–127, doi:10.1017/S1743921315006821
Larsen S. S., Brodie J. P., Huchra J. P., Forbes D. A., Grillmair C. J., 2001, AJ, 121, 2974
Li H., Gnedin O. Y., 2014, ApJ, 796, 10
Li H., Gnedin O. Y., 2018, preprint, (arXiv:1810.11036)
Li H., Gnedin O. Y., Gnedin N. Y., Meng X., Semenov V. A., Kravtsov A. V., 2017, ApJ, 834, 69
Li H., Gnedin O. Y., Gnedin N. Y., 2018, ApJ, 861, 107
Mandelker N., van Dokkum P. G., Brodie J. P., van den Bosch F. C., Ceverino D., 2018, ApJ, 861, 148
Marinacci F., Pakmor R., Springel V., 2014, MNRAS, 437, 1750
Monachesi A., et al., 2018, preprint, (arXiv:1804.07798)
Pakmor R., Springel V., 2013, MNRAS, 432, 176
Pakmor R., Marinacci F., Springel V., 2014, ApJ, 783, L20
Pakmor R., Springel V., Bauer A., Mocz P., Munoz D. J., Ohlmann S. T., Schaal K., Zhu C., 2016, MNRAS, 455, 1134
Peebles P. J. E., 2017, preprint, (arXiv:1708.04542)
Peng E. W., et al., 2006, ApJ, 639, 95
Pfeffer J., Kruijssen J. M. D., Crain R. A., Bastian N., 2018, MNRAS, 475, 4309
Prisinzano L., et al., 2018, arXiv e-prints, p. arXiv:1812.03025
Renaud F., Agertz O., Gieles M., 2017, MNRAS, 465, 3622
Schweizer F., 1987, in Faber S. M., ed., Nearly Normal Galaxies. From the Planck Time to the Present. pp 18–25
Springel V., 2010, MNRAS, 401, 791
Springel V., Hernquist L., 2003, MNRAS, 339, 289
Springel V., Di Matteo T., Hernquist L., 2005, MNRAS, 361, 776
Tonini C., 2013, ApJ, 762, 39
Tumlinson J., 2010, ApJ, 708, 1398
VandenBerg D. A., Brogaard K., Leaman R., Casagrande L., 2013, ApJ, 775, 134
Veljanoski J., Helmi A., 2016, A&A, 592, A55
Veljanoski J., et al., 2014, MNRAS, 442, 2929
Vogelsberger M., Genel S., Sijacki D., Torrey P., Springel V., Hernquist L., 2013, MNRAS, 436, 3031
Webb J. J., Reina-Campos M., Kruijssen J. M. D., 2018, arXiv e-prints, p. arXiv:1812.00014
Zick T. O., Weisz D. R., Boylan-Kolchin M., 2018, MNRAS, 477, 480
Zinn R., 1985, ApJ, 293, 424

APPENDIX A: SCATTER BETWEEN INDIVIDUAL AURIGA HALOES, AND NUMERICAL CONVERGENCE

We check whether the properties of the Auriga globular cluster candidates are well converged between the three different resolution levels used for the Auriga simulations. Here we consider all three Auriga haloes for which simulation runs were performed at all three resolution levels: Au6, Au16, and Au24. Here we can investigate differences between individual haloes.

Fig. A1 shows the mass-weighted metallicity distribution, Fig. A2 shows the mass-weighted radial distribution, and Fig. **??**

This paper has been typeset from a TEX/LATEX file prepared by the author.

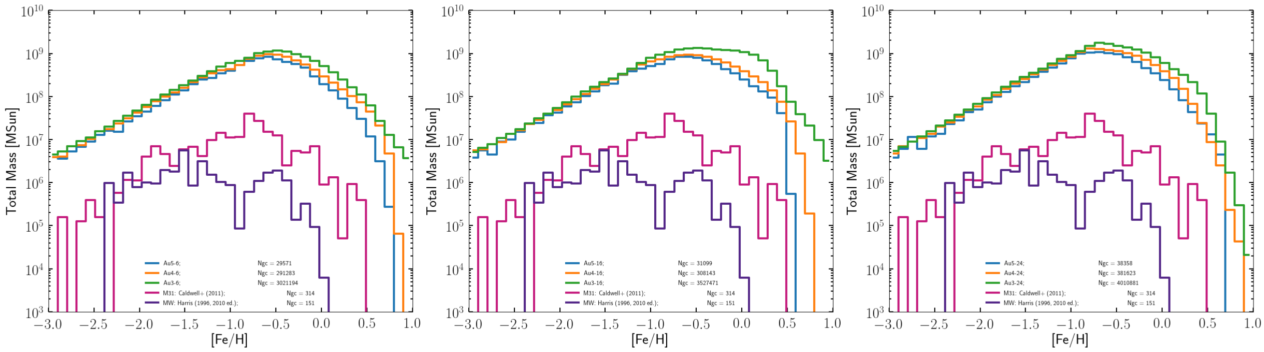

Figure A1. Same as Fig. 3, but here the colours indicate resolution level: L3 green, L4 orange, and L5 blue. *Left:* Auriga halo 6. *Mid:* Auriga halo 16. *Right:* Auriga halo 24. For all three haloes we find marginal increases in the mass normalization with increasing resolution level.

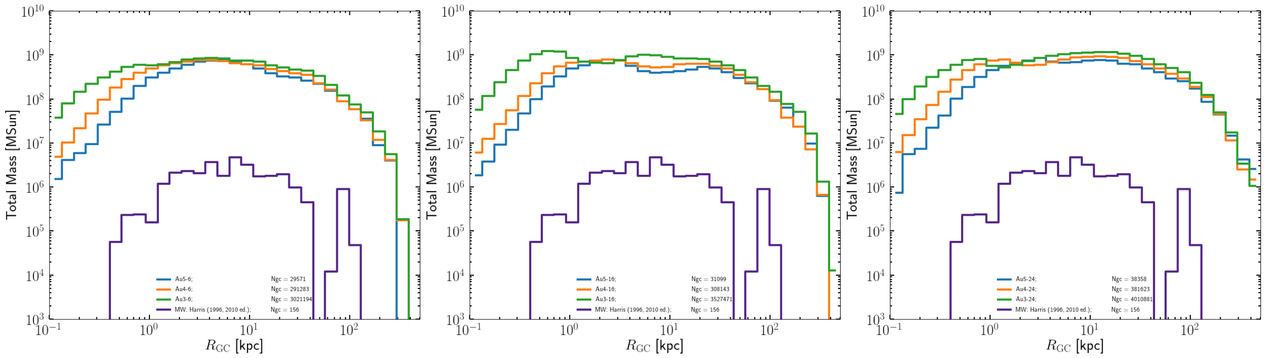

Figure A2. Same as Fig. 5, but here the colours indicate resolution level: L3 green, L4 orange, and L5 blue. *Left:* Auriga halo 6. *Mid:* Auriga halo 16. *Right:* Auriga halo 24. For all three haloes we find marginal increases in the mass normalization with increasing resolution level.